PAPER

Check for updates

Thermo-oxidative stability and flammability properties of bamboo/kenaf/nanoclay/epoxy hybrid nanocomposites

Siew Sand Chee,[a] Mohammad Jawaid, [ID] *[ab] Othman Y. Alothman[b] and Ridwan Yahaya[c]

In this study, three types of nanoclay [halloysite nanotube (HNT), montmorillonite (MMT) and organically modified MMT (OMMT)] were incorporated into bamboo/kenaf (B/K) reinforced epoxy hybrid composites to compare their thermo-oxidative (TOD) stability and flammability properties. B/K (50 : 50) hybrid nanocomposites were fabricated by adding 1% loading (by weight) nanoclay through a hand lay-up technique. Wide angle X-ray scattering (WAXS) and field emission scanning electron microscopy (FESEM) were used to study the morphology of the nanoclay–epoxy mixture. The TOD stability of the hybrid nanocomposites was studied with a thermogravimetry analyzer (TGA) under oxygen atmosphere. The flammability properties were evaluated using the Underwriters Laboratories 94 horizontal burning test (UL-94HB), limiting oxygen index (LOI), cone calorimetry and smoke density test. The morphological study reveals that MMT/epoxy and HNT/epoxy are highly agglomerated while OMMT/epoxy reveals a more uniform distribution morphology. The obtained results reveal that B/K/HNT shows better TOD stability below 300 °C, but B/K/MMT and B/K/OMMT show high residue content and decomposition temperatures above 300 °C. The flame retardancy of the hybrid nanocomposites improved with the loading of all types of nanoclay, but B/K/OMMT shows higher flame retardancy than B/K/MMT and B/K/HNT hybrid nanocomposites. Hybrid nanocomposites show improvement in flame properties in terms of peak heat release rate (pHRR), total heat release, fire growth rate index (FIGRA) and maximum average rate of heat emission (MARHE) and smoke growth rate index (SMOGRA) indicators. The findings from this work can be utilized to prepare high-performance fire retardant natural fiber reinforced epoxy hybrid composites for automotive and construction applications to save human lives.

Introduction

Polymer matrix composites are more favourable compared to metal and ceramic matrixes due to their low-cost production and easy construction. Substituting synthetic fibers with natural fibers has gained much attention from the research community and has taken a share in the world of composites. The natural fiber composites (NFCs) market is projected to support substantial growth over the forecasted years (2019–2024) with a compound annual growth rate (CAGR) of 10.93%.[1] The major driving force in the growing market of NFCs is the rising need for biocomposites in several industries, such as building and construction, automotive, aerospace and electronics. Despite

the growing demand for NFCs, their inherent properties of high flammability and releasing toxic gases during the combustion of both polymer matrix and natural fibers have greatly hindered their versatility in different applications.

Combustion is a complex physicochemical process between a flammable material and oxygen, accompanied by the emission of heat and light. In general, it consists of two salient processes, the transportation of mass and heat in both the gas and solid phases. First, the solid material decomposes to release volatiles into the boundary layer with the help of enough heat. These volatile gases then mix with surrounding oxygen to produce a flammable mixture and start the combustion cycle. Inflammable gases (CO_2, CO, NO), smoke, light and heat are generated during the combustion cycle. If the generated combustion heat is high enough to sustain the concentration of flammable volatiles, this process is regarded as self-continuous combustion.[2,3]

Flammability refers to the capability of ignition, flame spreading and heat generation. To improve the flammability properties of NFCs, fire retardants (FRs) were introduced into the composite system.[4] Halogenated FRs such as

[a]Laboratory of Biocomposite Technology, Institute of Tropical Forestry and Forest Products (INTROP), Universiti Putra Malaysia (UPM), 43400 Serdang, Selangor, Malaysia. E-mail: jawaid_md@yahoo.co.in

[b]Department of Chemical Engineering, College of Engineering, King Saud University, Riyadh, Saudi Arabia

[c]Science and Technology Research Institute for Defence (STRIDE), Kajang, Selangor, Malaysia

hexabromocyclododecane have been proved to effectively retard fire propagation and dominated the largest market share of FRs until the 1990s. However, regulations such as the Restriction of Hazardous Substances (RoHS) and the Waste Electrical and Electronics Equipment (WEEE) have limited the usage of halogenated FRs due to their potentially poisonous decomposition products, as well as their perseverance in the environment and bio-accumulation.[5] Alternatively, more eco-friendly non-halogenated FRs, such as metal hydroxides (aluminium hydroxide, magnesium hydroxide), inorganic fillers (calcium carbonate, silica, carbon black, *etc.*) and intumescent fire retardant systems (ammonium polyphosphate/pentaerythritol/melamine), were used to replace halogenated FRs.[6] Most studies showed that conventional FRs required high filler loading (>10%) to achieve effective fire retardant performance.[7,8] The high filler loading might lead to a secondary issue in which deterioration of the mechanical properties is often observed.[9]

Nanoscale particles, such as carbon nanotubes,[10,11] silica[12] and clay-based minerals,[5,13,14] have been gaining attention for use as FRs with a small loading level. Noteworthily, nanoscale filler is able to improve the fire behavior of a polymer composite without compromising its physical and mechanical properties. Montmorillonite (MMT) has been widely reported for use as a filler in the preparation of clay/polymer nanocomposites due to its abundance, environmental safety and well-understood chemistry.[15–17] MMT is a 1-dimensional nanofiller with a three-layer crystal sheet, consisting of two tetrahedral layers sandwiching an octahedral layer. Another type of nanoclay that has been heavily researched in the past few decades is halloysite nanotubes (HNTs). HNTs are a 1 : 1 phyllosilicate clay, consisting of a single tetrahedral sheet (Si–O) and an octahedral sheet (Al–OH), identical to kaolinite. HNTs are multiwalled inorganic nanotubes and offer an economical, low-tech option with a morphology comparable to multiwalled carbon nanotubes (CNTs). The fire retardancy mechanism of clay-base minerals is due to the development of a shielding barrier consisting of clay platelets that depletes the volatile products of thermal degradation.[18] It is known that well-dispersed nanoclay and the formation of intercalated/exfoliated nanocomposite are the key factors for enhancement of thermal stability and fire performance. Thus, surface modification on the nanoclay by using a suitable organic modifier with the aim to improve thermal and fire performance has been widely studied by researchers.[19–22]

Hybridizing natural fibers and nanoclay modified polymeric composites creates a potential alternative material with regards to environmental concerns. These new raised hybrid composites provide enhanced properties that cannot be obtained from either natural fiber composites or nanoclay/polymer composites. Hasan *et al.*[23] reported on the enhancement of the thermal stability property of jute/polyester composites with the addition of 5% OMMT. Shahroze *et al.*[24] also reported similar findings with sugar palm fiber/OMMT/polyester composites. Additionally, N. Saba *et al.*[25] explored the flammability property of kenaf/epoxy composites with the addition of MMT, OMMT and oil palm empty fruit bunch nanofiller. All hybrid nanocomposites exhibit better limiting oxygen index (LOI) and Underwriters Laboratories vertical burning test (UL-94V)

compared to kenaf/epoxy composites. Monteiro *et al.*[26] explore the fire behaviour of flax fiber and flax/carbon fiber phenolic based composites. The addition of nanoclay to the composites reduced the peak heat release rate (pHRR), mass loss rate and smoke generation.

The current study is a continuation of our previous work[27–29] which aims to prepare high-performance bamboo/kenaf reinforced epoxy hybrid nanocomposites with improvements in thermal stability and fire retardancy. In this work, bamboo/kenaf reinforced epoxy/nanoclay hybrid nanocomposites were prepared by a hand lay-up technique. A comparative study was carried out on three nanoclays (HNT, MMT and OMMT) with a fixed filler loading of 1% by weight. The thermo-oxidative stability of the fabricated hybrid nanocomposites was studied by TGA under an oxygen atmosphere. To gain insight into the flammability properties, the fabricated hybrid nanocomposites were tested using the Underwriter Laboratories 94 horizontal burning test (UL-94HB), limiting oxygen index (LOI), cone calorimetry and smoke density tester.

Materials and methods

Materials

DGEBA (diglycidyl ether of bisphenol-A) epoxy resin (DER-331, Dow Chemical Company) and JOINTMINE 905-3s amine hardener were supplied by Tazdiq Engineering Sdn. Bhd. (Selangor, Malaysia). The epoxy equivalent weight and amine value of the hardener are 182–192 g eq.$^{-1}$ and 300 ± 20 mg KOH per g, respectively. The unmodified montmorillonite (MMT), halloysite nanotubes (HNT) and organically modified MMT (OMMT, trade name Nanomer I.31PS) were all obtained from Sigma-Aldrich Malaysia and used as received. The specifications of the nanoclays are tabulated in Table 1. The non-woven bamboo mat and woven kenaf mat used in this study were supplied by Shijiangzhuang Bi Yang Technology Co. Ltd. (Hebei, China) and ZKK Sdn. Bhd. (Selangor, Malaysia), respectively. The specifications of the natural fibers are tabulated in Table 2.

Preparation of natural fiber reinforced epoxy/nanoclay hybrid nanocomposites

The epoxy/nanoclay mixture was prepared by *in situ* polymerization and the filler loading used in this study was fixed at 1 wt% in accordance with our previous work.[29] The nanoclay was weighed and dispersed slowly into the epoxy resin. The mixture was stirred slowly using a mechanical stirrer, followed by mixing with a high

Table 1 Specifications of MMT, HNT and OMMT used in this study

	MMT	HNT	OMMT
Mean particle size (μm)	≤25	—	14–18
Bulk density (kg m^{-3})	600–1100	—	250–300
Diameter (nm)	—	30–70	—
Length (μm)	—	1–3	—
Surface modifier (%):	—		
Octadecyl ammonium	—	—	15–35
3-Aminopropyltriethoxy silane	—	—	0.5–5

Table 2 Specifications of non-woven bamboo mat and woven kenaf mat

	Bamboo	Kenaf
Cellulose content (%)	72.6	65.7
Hemicellulose content (%)	11.1	17.8
Lignin content (%)	9.5	6.0
Unit area density (kg m^{-2})	0.8	0.6

shear speed homogenizer (T-25 Ultra Turrax Homogenizer, IKA). The mixture was subjected to a rotation speed of 10 000 rpm for 30 minutes in an ice bath to avoid excessive heat generation due to the high mixing speed. After being degassed for 30 minutes, the hardener was added slowly and mixed homogeneously by hand stirring. Finally, the epoxy/nanoclay mixture was ready to be used for the fabrication of fiber reinforced epoxy/nanoclay hybrid composites by hand lay-up technique. The total fiber loading used in this study is 40% and the mixing ratio of bamboo fiber to kenaf fibers is 50 : 50, chosen according to the outcomes from our previous studies.[28,30] The bamboo fibers and kenaf fibers were arranged layer by layer in a 240 mm × 120 mm × 3 mm stainless mold and then fibers mat impregnated with the prepared epoxy/nanoclay mixture. A hand roller was used to remove air bubbles that might present on the laminates. The mold was left at room temperature to cure for 24 hours followed by post-curing at 105 °C for 5 hours to ensure full curing. The same method was used to fabricate unfilled bamboo/kenaf reinforced epoxy hybrid composite as a control sample.

Characterization

Morphology. Wide angle X-ray scattering (WAXS) analysis was used to evaluate the basal spacing (d-spacing) between the clay layers.[31,32] The WAXS measurements were performed using an Anton Paar Saxpoint 2.0 diffractometer with Cu-Kα radiation (wavelength = 0.1542 nm) under a voltage of 50 kV and current of 1 mA. The d spacing was calculated according to Bragg's Law as per eqn (1).

$$d \text{ spacing } (d001) = \frac{n\lambda}{\sin 2\theta} \quad (1)$$

Here, n is order 1, λ is the Cu-Kα radiation wavelength used, and 2θ denotes the peak position, which corresponds to the 001 basal reflection peak of the interlayers. The dispersion and aggregation of the nanoclay in the epoxy matrix were studied by field emission scanning electron microscopy (FESEM). The FESEM images were obtained by using a FEI Nova NanoSem 230 instrument.

Thermo-oxidative stability. The thermo-oxidative stability of the nanoclay and hybrid nanocomposites were measured with a Mettler Toledo thermogravimetry analyzer (Model: TGA 1) according to ASTM E1131-03 (2003). The analysis was carried out from 25 °C to 800 °C at a heating rate of 20 °C min^{-1} under an oxygen atmosphere (oxygen flow rate = 50 ml min^{-1}).

Underwriters Laboratories 94 horizontal burning test (UL-94HB). The test employed in this study is horizontal burning which is technically equivalent to ASTM D635 (rate of burning

and/or extent and time of burning of plastics in a horizontal position). A bar specimen with dimensions of 125 mm × 13 mm × actual thickness of specimen (≤13 mm) was prepared and supported horizontally at one end. The free end was subjected to the flame and the flame was removed from the specimen after 30 s. The timer was started when the flame hit the first gauge length (25 mm) and the elapsed time for the flame to travel from the 1st gauge mark (25 mm) to the 2nd gauge mark (100 mm) was recorded in seconds (t) and the burn length (L) was recorded as 75 mm. The total elapsed time for the flame to move from the 1st gauge mark to the 2nd gauge mark was recorded and the linear burning rate (V) was calculated according to eqn (2).

$$V \text{ (mm min}^{-1}) = L/t \, (60) \quad (2)$$

Here, L = the burned length (75 mm) and t = the elapsed time in seconds for the burning from the 1st gauge mark to the 2nd gauge mark.

Limiting oxygen index. LOIs of the specimens were tested according to ASTM D2863. A Type IV specimen size was prepared with dimensions of 100 mm × 6.5 mm × 3 mm. The specimen was ignited like a candle following ignition procedure A (top surface ignition). Each group of hybrid nanocomposites consisting of a set of 15 specimens was tested until the last 5 tested specimens obtained a deviation of 0.2 vol% in oxygen concentration. Based on the last 5 test specimens' burning pattern, the final LOI is calculated as per eqn (3).

$$\text{LOI (vol\%)} = C_F + kd \quad (3)$$

Here, C_F is the final value of oxygen concentration in vol% to one decimal place used in the series of the last 5 measurements, d is the interval difference between the oxygen concentration levels in percent volume (0.2 vol%), and k is a factor obtained from Table 2 as described in ASTM D2863.

Cone calorimetry test. The flammability properties such as time to ignition (TTI), peak heat release rate (pHRR), total heat release rate (THR) and mass loss rate (MLR) were determined according to ISO 5660 using a cone calorimeter (Fig. 1(a)) supplied by Fire Engineering & Science Technology (FESTEC International, Korea). Specimens with dimensions of 100 mm × 10 mm × actual sample thickness were prepared. The
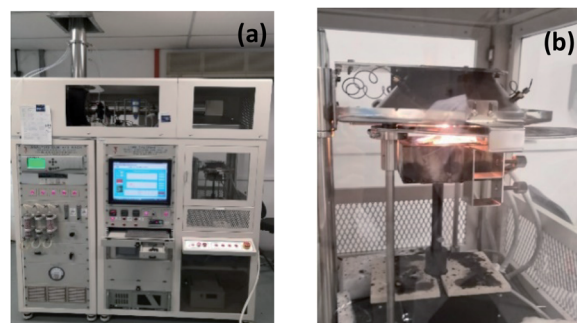

Fig. 1 (a) Cone calorimeter tester; (b) combustion process after spark ignition.

Paper

specimens were wrapped on the side and bottom with aluminium foil and then placed horizontally on the sample holder. The surface of the specimens was subjected to spark ignition and irradiated with 35 kW m^{-2} heat flux (Fig. 1(b)).

Smoke density. The optical density of smoke was assessed according to ASTM E662 using a smoke density tester (SB501, FESTEC International, Korea). Each specimen with a dimension of 75 mm × 75 mm × actual sample thickness was covered in aluminium foil and exposed vertically to a heat flux of 25 kW m^{-2} without the application of a pilot flame. A light beam was then shone through the chamber. The smoke density can subsequently be calculated by measuring the obscuration of the light beam by the smoke using a photosensor. VOF 4 refers to the total of the optical densities measured in the first 4 min of the sample exposure to heat flux and is calculated as per eqn (4).

$$\text{VOF } 4 = \text{SD}_{1\text{ min}} + \text{SD}_{2\text{ min}} + \text{SD}_{3\text{ min}} + (\text{SD}_{4\text{ min}}/2) \qquad (4)$$

Here $\text{SD}_{1\text{ min}}$, $\text{SD}_{2\text{ min}}$, $\text{SD}_{3\text{ min}}$ and $\text{SD}_{4\text{ min}}$ are the values of the specific optical densities recorded at the 1st, 2nd, 3rd and 4th minutes, respectively.

Results and discussion

Structural and morphological study on nanoclay/epoxy composites

Fig. 2(a) shows the WAXS curves obtained for the OMMT, MMT and HNT nanoclay powders and Fig. 2(b) displays the WAXS curves for the corresponding nanoclay/epoxy composites. The recorded 2θ peaks and their calculated d spacings are tabulated in Table 3. The 2θ peaks observed for MMT, HNT and OMMT powders were recorded at 6.56°, 13.28° and 4.34°, respectively. The calculated interlayer spacing for MMT is 1.35 nm while the d spacing for HNT is 0.67 nm; these findings well match the characteristics of the 2 : 1 phyllosilicate (smectite)[33] and 1 : 1 phyllosilicate (kaolin) types.[34] OMMT recorded the highest d spacing among the nanoclays at 2.04 nm due to the interaction between the unmodified MMT and the surface modifiers (alkylammonium/silane) expanding the clay layer distance. Polymer monomer diffused into the expanded clay galleries resulting in shifting the 2θ peak lower.[29] However, the d spacing remaining nearly identical to the pristine state suggests that polymer monomer hardly penetrated the clay layers and a resulting immiscible dispersion is formed.[35] We observed in HNT/epoxy that the recorded d spacing (0.72 nm) is almost identical to its pristine state (0.67 nm), while MMT/epoxy recorded a slight increase in d spacing from 1.35 nm to 1.78 nm.

OMMT/epoxy recorded the largest d spacing at 2.54 nm. The morphology of the nanocomposites was further confirmed with FESEM (Fig. 3). Analysis of FESEM allows observation of the presence of filler and agglomerates on the surfaces of fractioned objects. The FESEM image of MMT/Epoxy nanocomposites under 16 000 times magnification shows large tactoid particles and agglomeration formation. A similar observation was made on HNT/epoxy nanocomposites, where stacking of HNTs was observed under 25 000 times magnification. In contrast, MMT/
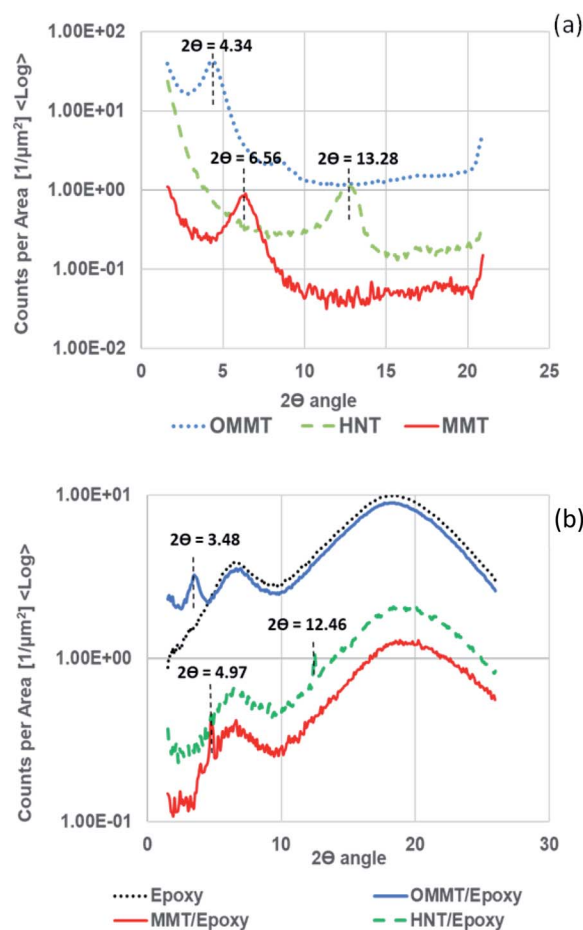

Fig. 2 (a) WAXS patterns of the MMT, HNT and OMMT powders; (b) WAXS patterns of epoxy, OMMT/epoxy, MMT/epoxy and HNT/epoxy composites.

Table 3 2θ peaks of WAXS curves and the corresponding d spacing of nanoclay powders

Specimens	Peak in 2θ (°)	d spacing (nm)
MMT	6.56	1.35
HNT	13.28	0.67
OMMT	4.34	2.04
MMT/epoxy	4.97	1.78
HNT/epoxy	12.46	0.72
OMMT/epoxy	3.48	2.54

epoxy revealed more uniform dispersion under 100 000 times magnification.

Thermo-oxidative decomposition behavior of bamboo/kenaf reinforced nanoclay/epoxy hybrid nanocomposites

The TGA analysis was carried out under an oxygen atmosphere to understand the thermo-oxidative decomposition (TOD) behavior of the nanoclays and hybrid nanocomposites. The decomposition mechanism of materials is greatly influenced by the atmosphere used in TGA analysis.[28,36] Thermal decomposition behavior
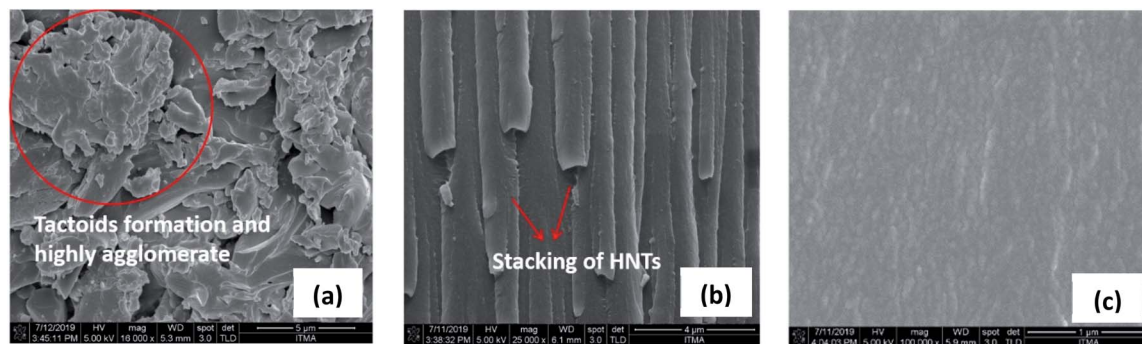
Fig. 3 (a) FESEM image of MMT/epoxy; (b) FESEM image of HNT/epoxy; (c) FESEM image of OMMT/epoxy.
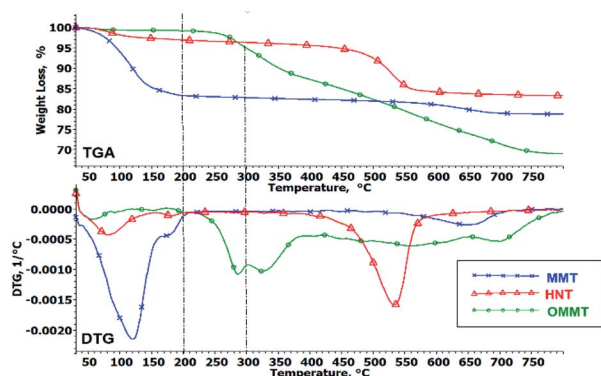

Fig. 4 TGA and DTG curves of MMT, HNT and OMMT powders measured under oxygen atmosphere.

Table 4 Decomposition profiles of nanoclay powders under oxygen atmosphere

Nanoclay	Temperature range (°C)	Weight loss (%)	Possible reaction
MMT	30–200	16.7	Moisture evaporation
	450–650	11.0	Dehydroxylation of clay layers
HNT	30–200	3.09	Moisture evaporation
	500–750	3.16	Dehydroxylation of clay layers
OMMT	30–200	0.76	Moisture evaporation
	200–300	4.32	Decomposition of APTES
	300–800	25.5	Decomposition of ODA

measured under oxygen atmosphere provide more pragmatic information for a real fire situation compared to measurements conducted under an inert atmosphere. Fig. 4 illustrates the TOD curves of MMT, HNT and OMMT powders. The details of the decomposition profile are tabulated in Table 4. The first weight loss step observed under 200 °C for all three nanoclays is related to moisture vaporization. MMT has the highest moisture content among the nanoclays (16%) due to its naturally hydrophilic characteristic, followed by HNT (3%) and OMMT (0.8%). This shows that surface modification changes the hydrophilic characteristics of the nanoclay and significantly reduces the moisture content. Both MMT and HNT reveal a subsequent weight loss step

in a higher temperature range (>400 °C) which can be related to dehydroxylation of the clay layer.[37,38] OMMT reveals a different oxidative decomposition profile compared to unmodified MMT. The second weight-loss step observed at a much lower temperature, around 200–300 °C, can be correlated to the decomposition of 3-aminopropyltriethoxysilane (APTES).[29] The DTG curve reveals that there is a third weight loss step from 300 °C onwards, gradually decreasing until 800 °C. This may be attributed to the decomposition of octadecylamine (ODA). Initially, the degradation of the ammonium salt produces a long carbon chain with an amine group; further breakdown of the long carbon chain forms short and long carbon alkenes.[39,40]

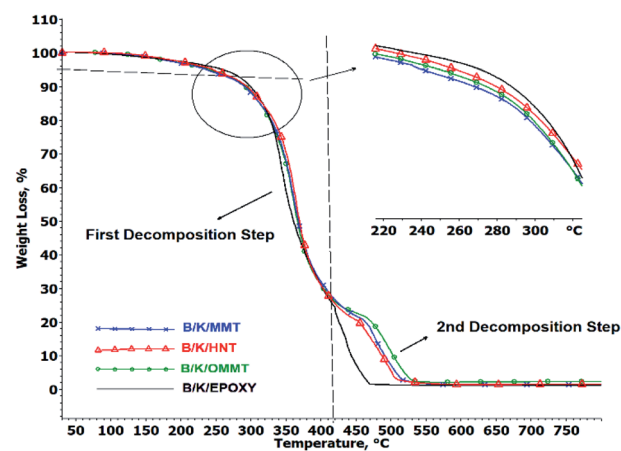The TOD curve of the hybrid nanocomposites is presented in Fig. 5 and the TGA data are summarized in Table 5. The TOD

Fig. 5 TGA curves of hybrid nanocomposites under oxygen atmosphere.

Table 5 Thermo-oxidative stability data of hybrid nanocomposites measured under oxygen atmosphere

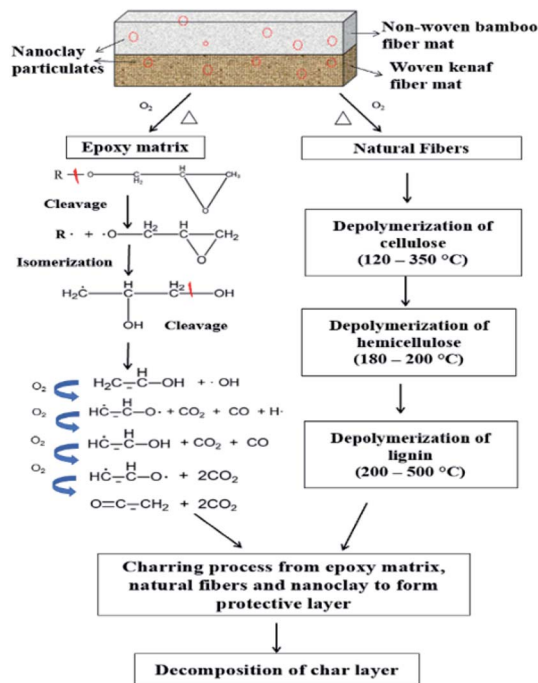| Hybrid composites	$T_{10\%}$ (°C)	T_{max1} (°C)	T_{max2} (°C)
B/K/MMT	289	356	485
B/K/HNT	297	365	483
B/K/OMMT	292	360	495
B/K/epoxy	299	346	434

Fig. 6 Schematic presentation of the decomposition process of bamboo/kenaf reinforced epoxy/nanoclay hybrid nanocomposite.

curves of all the hybrid nanocomposites reveal two weight loss steps with the initial weight loss step observed around 250–400 °C and a subsequent weight loss step occurring around 400–550 °C. The first and second decomposition steps are represented by T_{max1} and T_{max2} as the temperatures of mass loss at the maximum rate.

The oxidative decomposition process of the bamboo/kenaf reinforced nanoclay/epoxy hybrid nanocomposites is a complex reaction involving decomposition of the different constituents in the hybrid nanocomposite system, as illustrated in Fig. 6. In general, the decomposition process involves decomposition of the epoxy matrix and the natural fibers, which happens around the first decomposition step (250–400 °C). Under a heat source, oxidation degradation occurs on the superficial layer of the polymer matrix, causing composite shrinkage and microcracking. Oxygen now easily diffuses into the specimen through the cracks and leads to further degradation. According to the degradation of epoxide by Neiman's scheme,[41] epoxy resin breaks down in several stages, forming free radical species that can further react with oxygen to generate hydroxyl free radicals.[41,42] This is an important process for sustaining the burning of the composite and contributes to the development of heat and flame.[2] Natural fibers undergo TOD through 3 major processes: thermo-oxidation, dehydration and depolymerization.[36] The initial depolymerization happens in hemicellulose in the temperature range of 120–200 °C. Hemicellulose mainly contains low molecular weight polysaccharides such as hexoses, pentoses and uronic acid. Concurrently, depolymerization of cellulose takes place in the temperature range of 180–350 °C, leading to the formation of glycosane.[43] Thermal decomposition of lignin happens over a broad temperature range (200–500 °C). This is attributed to the

different oxygen functional groups on its structure decomposing at different temperatures.[44,45] The charring process is an intermediate stage of the TOD process. Oxygen reacts with the decomposing condensed phase, forming a thermally stable char layer. Subsequently, when the temperature rises high enough to increase the reaction rate between the condensed phase and oxygen, the char layer decomposes. This can explain the observation of the second decomposition step in the TGA curves.

The initial decomposition temperature is represented by $T_{10\%}$ (Table 5). We observed that the initial decomposition temperatures of all hybrid nanocomposites are lowered compared to B/K/epoxy. The $T_{10\%}$ of B/K/MMT, B/K/HNT, B/K/OMMT and B/K/Epoxy are recorded at 289 °C, 297 °C, 292 °C and 299 °C, respectively. This may be due to the incorporation of unmodified MMT and HNT leading to poor dispersion and a heterogeneous morphological structure in the hybrid nanocomposites. The agglomerated particulates may hinder the migration of the nanoclay to the surface, thus preventing it from forming an effective protective barrier against the heat and volatiles and resulting in lower initial decomposition temperatures.[18] Another possible reason for this observation is the relatively high moisture contents in MMT (16.7%) and HNT (3.09%) could cause an excessive amount of trapped volatiles during heating. This leads to high internal pressure during escape, thus increasing void formation and microcracks that can cause earlier degradation. In the case of B/K/OMMT, the lowering of the initial decomposition temperature can be ascribed to the decomposition of the organic modifier ($\geq$200 °C), as discussed earlier. Furthermore, the Hoffman degradation mechanism of the alkyl ammonium salt attached to the OMMT clay can act as a protonic acid catalyst and promote the degradation of the polymer matrix.[35,46]

With the addition of nanoclay, the thermal stability is enhanced by: (i) forming a protective layer on the surface of the polymer during heat and fire contact and (ii) catalyzing and reinforcing char creation.[18] As the temperature increases above 300 °C, nanoclay filled hybrid nanocomposites show higher thermal stability compared to B/K/epoxy. B/K/HNT recorded the highest T_{max1} (365 °C), followed by B/K/OMMT (360 °C) and B/K/MMT (356 °C). Finally, the recorded T_{max1} for B/K/epoxy is
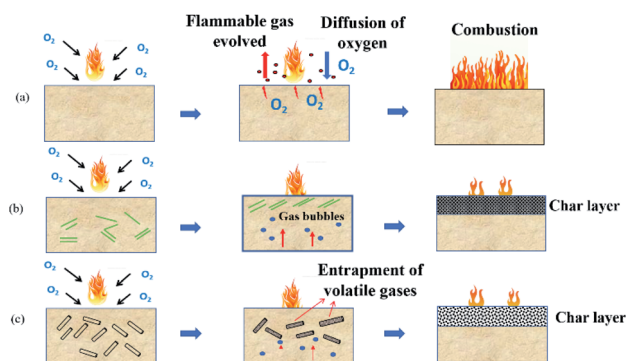

Fig. 7 Schematic presentation of the combustion process and char protection mechanism of hybrid composites: (a) B/K/epoxy, (b) B/K/OMMT, (c) B/K/HNT.
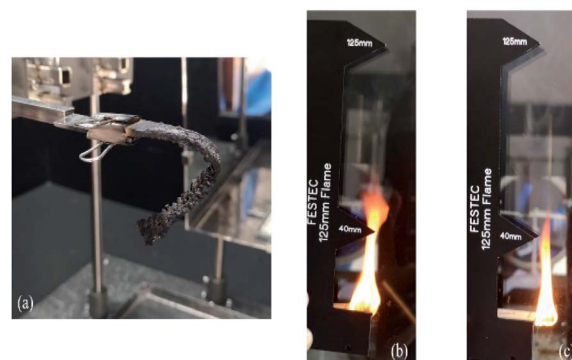
Table 6 Oxidation char residue recorded at 450 °C, 500 °C, 550 °C and 800 °C

Hybrid composites	Residue content, %			
	450 °C	500 °C	550 °C	800 °C
B/K/MMT	21.9	7.13	1.81	1.54
B/K/HNT	20.7	5.42	1.73	1.43
B/K/OMMT	22.8	11.1	2.21	1.92
B/K/epoxy	7.36	1.38	0.64	0.52

346 °C. During the decomposition process, migration and accumulation of the nanoclay at the composite surface is driven by the formation of rising gas bubbles, thermodynamic effects, and the temperature and viscosity gradients within the composite.[47,48] The formation of the silicate char layer provides heat and flame insulation, thus protecting the polymer surface from the flame zone for further thermal oxidation reaction. Additionally, the protective barrier also will slow the outgoing flammable volatiles and diffusion of oxygen into the composite. In the case of B/K/HNT, besides the protective char mechanism, the thermal stability of the hybrid nanocomposites is also enhanced by the entrapment mechanism of HNT. It has been reported that tubular HNT has a length of 2–40 μm and outer and inner diameters between 20–190 nm and 10–100 nm, respectively.[49] A degradable compound can be trapped inside the lumen, which delays mass transfer to the flame zone, thus improving the thermal properties of the composite.[50,51] This explains the higher T_{max1} in B/K/HNT compared to B/K/MMT observed in this current study. Fig. 7 illustrates the protective mechanism induced by OMMT and HNT in the composite system. In contrast, the organic modifier in B/K/OMMT degrades gradually at a higher temperature; the decomposition of the organic modifier accelerates the migration of the nanoclay towards the exposed surface. Also, the silicate clay layers provide a more difficult pathway and hinder the mass transfer (volatile combustible and oxygen transfer), resulting in higher thermal stability compared to B/K/MMT. Similar observations have been previously reported.[25]

The complete oxidation-combustion of the char layer is characterized by T_{max2}. The char residue contents recorded at 450 °C, 500 °C, 550 °C and 800 °C are tabulated in Table 6. B/K/OMMT recorded the highest char decomposition temperature (T_{max2}) and the highest char residue among the composites. The T_{max2} of B/K/OMMT was recorded at 495 °C and is 60 °C higher compared to B/K/epoxy. This indicates that B/K/OMMT exhibits the best catalyzing effect and accelerated char formation, displaying a more complex, compact, stable and dense

Fig. 8 (a) Hybrid composites after horizontal UL-94 burning test, (b) estimated flame height produced by B/K/Epoxy, (c) estimated flame height produced by B/K/OMMT.

carbonaceous structure. The hybrid composites filled with MMT and HNT decompose at lower temperatures compared to B/K/OMMT, with their T_{max2} values recorded at 485 °C and 483 °C, respectively. Eventually, the char layer oxidizes completely, leaving a minimal residue value. The residue values of the hybrid nanocomposites at 800 °C are significantly increased by 196%, 175% and 269% with the additions of MMT, HNT and OMMT nanoclays, respectively.

UL-94 horizontal burning test (UL-94HB)

UL-94 refers to the "Standard for Tests for Flammability of Plastic Material for Parts in Devices and Appliances", released by Underwriters Laboratories of the United States.[52] The horizontal burning (HB) test of UL-94 is employed in the current study to determine the HB flammability rating of the hybrid nanocomposites. The HB test assesses the burning rate of a specimen in mm min^{-1} with respect to its thickness and gives insight on the ignitability and flame spread characteristics of the material. Table 7 tabulates the observations and data obtained from the UL-94 HB tests. All specimens show continuous burning characteristics in which the flame was able to pass the 1st and 2nd gauge marks without extinguishing.

Flame dripping was not observed on any type of hybrid composite. This is probably due to the mat-form reinforcing fibers used in this study, which provide better structural integrity. Evidence of this can be observed in the photo (Fig. 8(a)) of a specimen after the UL-94HB test. There is also evidence that the incorporation of nanoclay delays the flame spread characteristic with a reduced linear burning rate. All specimens obtained a flammability rating of HB 40, indicating their linear burning rate is ≤40 mm min^{-1} with respect to their

Table 7 Observations and data obtained from UL94 horizontal burning test according to ASTM D653

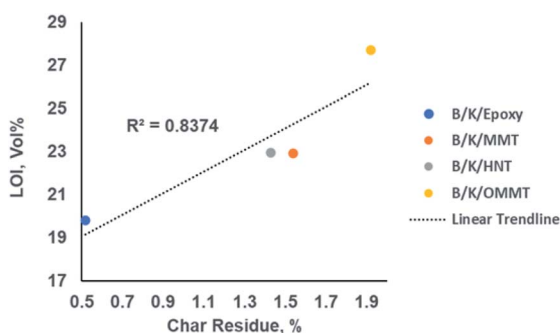| Composites	Dripping	Time from 1st gauge mark to 2nd gauge mark (s)	Linear burning rate (mm min^{-1})	Rating
B/K/epoxy	No	353.0 ± 3.9	12.7	HB40
B/K/MMT	No	382.2 ± 6.2	11.8	HB40
B/K/HNT	No	372.2 ± 3.0	12.1	HB40
B/K/OMMT	No	455.0 ± 4.2	9.89	HB40

Table 8 Data obtained for LOI testing for hybrid nanocomposites according to ASTM D2863

Composites	C_F (°C)	k	d (°C)	LOI (%)	Standard deviation
B/K/epoxy	19.4	2	0.2	19.80	0.24
B/K/MMT	22.8	0.61	0.2	22.92	0.42
B/K/HNT	22.8	0.68	0.2	22.94	0.32
B/K/OMMT	27.8	−0.45	0.2	27.71	0.13

sample thickness, which falls between 3–4 mm. The linear burning rate of the hybrid composites follows the sequence of B/K/epoxy > B/K/HNT > B/K/MMT > B/K/OMMT. In addition, we also observed that the flame height of the nanoclay filled hybrid composites is lower compared to the unfilled hybrid composite (Fig. 8(b) and (c)). The delay of flame spread in the hybrid nanocomposites can be ascribed to the formation of the protective carbonaceous layer which acts as a heat and flame insulator, limiting the outgoing volatile gases and the diffusion of oxygen into the material.[47] In the case of the hybrid nanocomposite filled with OMMT, the content of organic modifier enhances the catalytic effect during the charring process, resulting in denser and more cohesive char formation.[53] Similar findings have also been reported by other researchers.[25,53,54]

Limiting oxygen index (LOI)

LOI is one of the fire indexes widely used to characterize the flammability of polymer materials, describing the lowest oxygen concentration needed to support flaming combustion of a material. The data are recorded in Table 8. The LOI value of B/K/epoxy is 19.80% and it is classified as combustible, as its LOI value is lower than air oxygen content (21%). All three types of nanoclay filled hybrid nanocomposite are classified as self-extinguishing, as their LOI values are greater than 21%. This indicates that the addition of nanoclay improves the flame retardant property whereby the combustion process cannot maintain itself at ambient temperature without an external heat source.[52] Incorporation of MMT and HNT nanoclays improved LOI values from 20% to 23% while the addition of OMMT improved the LOI from 20% to 28%. In addition, van Krevelen[55] reported a linear correlation between the char residue and LOI.
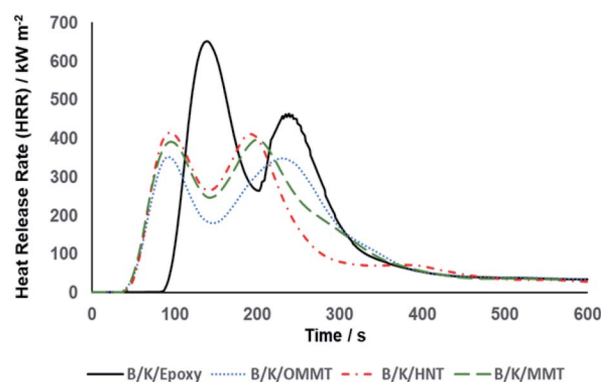
The LOI values of hybrid composites increase with their ability to yield char in a fire. Our findings in this work are in line with this observation, as illustrated in Fig. 9. A relatively high correlation coefficient, $R^2 = 0.8374$, is obtained between the LOI value and char residue at 800 °C from TGA analysis. This is due to the greater amount of char formation reducing the emission of flammable volatiles; as a result of this, the oxygen level needed to maintain flaming combustion is increased.[55,56]

Cone calorimetry

The combustion behaviour of the hybrid nanocomposites was investigated by cone calorimetry, which gathers data such as time to ignition (TTI), heat release rate (HRR), mass loss rate (MLR) and other parameters correlated with the fire behaviour of the samples (Table 9). TTI characterizes the time required for ignition when the material is exposed to a constant heat flux (35 kW m^{-2}) under an oxygen-controlled environment. It reflects how soon the surface of the material reaches pyrolysis temperature and the production of the flammable volatile gases required to sustain the flame over the whole sample surface.[12,57] Thus, a higher TTI is more favourable and deemed to be less flammable. However, the TTI values of all the nanoclay filled hybrid nanocomposites are shorter compared to B/K/epoxy. B/K/MMT recorded the lowest TTI (32 s), followed by B/K/OMMT (45 s) and B/K/HNT (46 s). B/K/epoxy recorded the highest TTI at 95 s. This may be attributed to the agglomerated clay cluster near the surface of the composites absorbing more heat through heat radiation and inducing higher thermal conductivity which then catalyses the polymer decomposition.[58,59] Of the two hybrid nanocomposites filled with unmodified nanoclay, B/K/HNT shows relatively higher TTI compared to B/K/MMT. This could be related to the entrapment mechanism of the volatile gasses in the hollow structure of HNT. In the case of B/K/OMMT, the organic modifier used for surface treatment decomposes at a lower temperature, thus reducing the TTI. These observations are consistent with the TGA analysis and similar observations reported by other researchers.[58,60]

Another important and critical parameter to characterize the flammability of a material is the heat release rate (HRR). HRR is

Fig. 9 Correlation between LOI value and char residue content of the hybrid nanocomposites at 800 °C.

Fig. 10 Heat release rate curves as a function of time for filled and unfilled bamboo/kenaf reinforced epoxy hybrid composites at 35 kW m^{-2} heat flux.

defined as the quantity of heat released per unit area of a material when the material is subjected to a fire and is expressed in kW m^{-2}. It is not only an important parameter to characterize fire behaviour but also serves as a determining factor in defining phenomena such as fire hazard. The generation of smoke, hazardous gases and other types of fire hazards increase in parallel with the HRR. Fig. 10 illustrates the HRR curves of the hybrid composites. We observed that all hybrid composites exhibit two peaks in the HRR curves. The first peak corresponds to the charring process forming the carbonaceous char structure. The char layer acts as a protective barrier that restricts the transportation of mass and volatiles between the condensed and gas phases. As a result, the combustion rate reduced and a decline in the HRR curves was observed after the occurrence of the first peak. As the burning continued, an excessive amount of trapped volatiles induced high internal pressure during escape, thus increasing void formation. This led to cracking and degradation of the char residue and further promoted combustion, creating another HRR peak. A similar argument has been made previously.[18,61] Peak HRR (pHRR) refers to the highest amount of heat emitted during combustion and the area under the HRR curve represents the total heat release (THR). The pHRR of B/K/epoxy recorded the maximum value of 680 kW m^{-2} and the highest total heat release (THR) of 103 MJ m^{-2} among all the composites. A significant reduction of pHRR between 36–43% was observed for nanoclay filled hybrid composites. Maximum reduction was observed on B/K/OMMT, with pHRR recorded at 388 kW m^{-2} and a THR of 83 MJ m^{-2}. This was followed by B/K/MMT and B/K/HNT with pHRRs at 414 kW m^{-2} and 432 kW m^{-2}, respectively, and THRs at 92 MJ m^{-2} and 101 MJ m^{-2}, respectively. The reduction of pHRR and THR in the hybrid nanocomposites compared to the unfilled hybrid composite represents char enhancement and improved thermal stability.[62]

It is not pragmatic to rely on just one parameter to validate the fire behaviour of a material. Thus, fire indexes such as FIGRA (fire growth rate index) and MARHE (maximum average rate of heat emission) have been used to define the fire performance of a material.[63] FIGRA is defined as the ratio of pHRR and the time to reach pHRR. It can be used to predict the fire magnitude as well as flame spread.[60,64] MARHE is defined as the peak value of the accumulative heat emission divided by time. It provides insight into the tendency for fire spread or development under a real fire scenario.[64] In order to reflect the flame retardancy of material, both indices should be at low values. From Table 9, we observe that all the nanoclay filled hybrid composites show reductions in both indices compared to unfilled hybrid composites, indicating better flame retardant performance. Mass loss rate (MLR) provides information on the physical changes by means of the composite degradation and char yield. L. Ahmed *et al.*[63] proposed to involve parameters such as pHRR, THR and average mass loss rate (MLR$_{AVG}$) to better interpret the flame retardant performance of a material. Fig. 11 illustrates the plot of pHRR as a function of THR $\times$ MLR$_{AVG}$ of the filled and unfilled hybrid composites.

It is observed that all filled hybrid nanocomposites exhibit lower pHRRs at lower THR $\times$ MLR$_{AVG}$ compared to the unfilled

Table 9 Cone calorimetry data for filled and unfilled bamboo/kenaf reinforced epoxy hybrid composites[a]

Composites	Time to ignition (s)	pHRR (kW m^{-2})	Total heat release (MJ m^{-2})
B/K/epoxy	95 (4.9)	680 (40)	103 (4)
B/K/MMT	38 (2.2)	414 (21)	92 (5)
B/K/HNT	46 (4.0)	432 (20)	101 (6)
B/K/OMMT	45 (1.7)	388 (35)	83 (7)

Composites	MLRAVG (g s^{-1} m^{-2})	FIGRA (W m^{-2} s^{-1})	MARHE (kW m^{-2})
B/K/epoxy	6.32 (2.5)	5765 (697)	273 (12)
B/K/MMT	4.59 (1.5)	4373 (126)	243 (8)
B/K/HNT	5.62 (1.3)	4591 (293)	251 (11)
B/K/OMMT	2.89 (1.8)	4072 (239)	232 (21)

[a] The values in parentheses are the standard deviations.

hybrid composite. It is apparent that B/K/OMMT reveals the best fire retardant performance among all hybrid composites, with the lowest peak heat release, lower MLR$_{AVG}$ (slow burning rate) and lower fire load for THR. B/K/MMT and B/K/HNT exhibit relatively lower flame retardant performance compared to B/K/OMMT but better flame retardant performance compared to B/K/epoxy. This probably is due to the poor dispersion and interaction between the unmodified nanoclay and epoxy resin. However, there are no distinct differences observed between the hybrid composites filled with MMT and HNT.

Smoke property

Smoke is a combination of particulates and non-particulates, comprising soot and organic compounds, emitted during the combustion of a material. Smoke emission during a fire scenario plays an important role in life safety due to its toxicity and reduced visibility. From the cone calorimetry test, several important smoke properties, such as total smoke production (TSP), smoke growth rate index (SMOGRA) and average specific
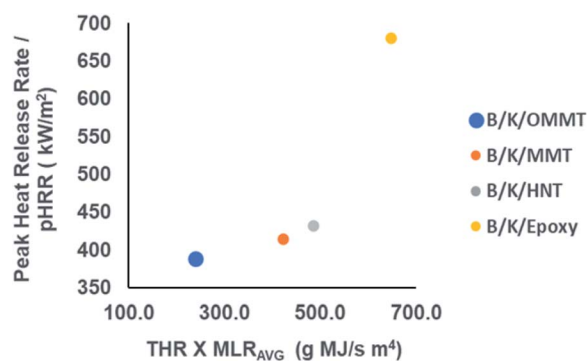

Fig. 11 Plot of pHRR as a function of THR $\times$ MLR$_{AVG}$ to evaluate fire retardant performance of filled and unfilled bamboo/kenaf reinforced epoxy hybrid composites.

Table 10 Smoke emission properties of filled and unfilled bamboo/kenaf reinforced epoxy hybrid nanocomposites[a]

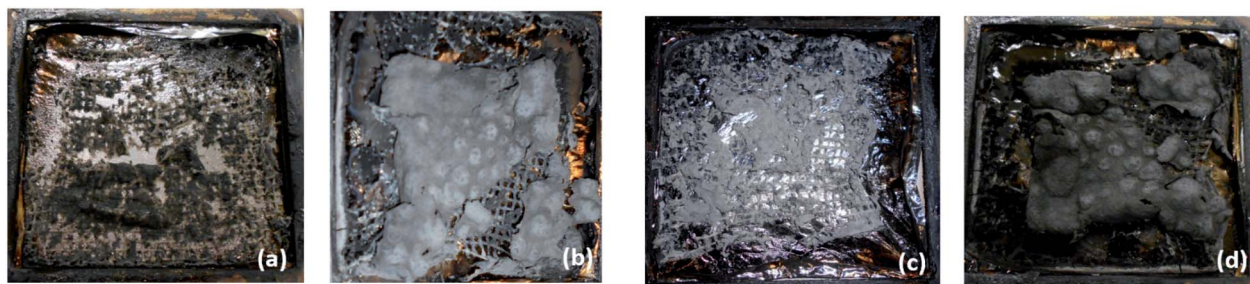| Composite	Cone calorimeter			Smoke density
	TSP (m^2)	SMOGRA ($m^2 \ s^{-2}$)	SEA_{AVG} ($m^2 \ kg^{-1}$)	VOF4
B/K/epoxy	2827 (284)	10.5 (1.46)	305 (41)	573
B/K/MMT	2289 (102)	9.17 (0.05)	219 (6)	180
B/K/HNT	2620 (137)	9.64 (0.19)	280 (13)	256
B/K/OMMT	1833 (156)	8.91 (0.05)	168 (42)	148

[a] The values in parentheses are the standard deviations.

Fig. 12 Photographic images of B/K/epoxy hybrid composite and B/K/epoxy hybrid nanocomposites after cone calorimetry tests: (a) B/K/epoxy, (b) B/K/MMT, (c) B/K/HNTT and (d) B/K/OMMT.

extinction area (SEA_{AVG}), were obtained and are summarized in Table 10. TSP and SMOGRA are classification parameters used to define the volume of smoke produced and were widely adopted by the Euroclass system in 'Single Burning Item test EN 13823'. Overall, we observed a better smoke suppression property in nanoclay filled hybrid composites compared to unfilled hybrid composite. The lowest TSP value is observed in B/K/OMMT followed by B/K/MMT, B/K/HNT and B/K/epoxy, with their TSP values at 1833 m^2, 2289 m^2, 2620 m^2 and 2827 m^2, respectively. Similar findings were also observed for SMOGRA values. It has been proposed that during continuous heating, clay migrates to the surface, forming a protective carbonaceous-silicate char layer that limits the mass transport of oxygen and volatile products.[65] This results in lower smoke production.

Average specific extinction area (SEA_{AVG}) allows us to gain insight into visibility during the fire scenario. During the cone calorimetry combustion test, the smoke flows through the analysis chamber together with additional gas flow. SEA is a parameter corresponding to the light absorption by the surface of smoke particles generated during burning of 1 kg of substance.[58] In addition, the smoke density tester provides information on the change of optical density of smoke accumulation in a closed chamber throughout the test period. In terms of SEA_{AVG} and VOF 4, the nanoclay filled hybrid composites again showed lower values compared to the unfilled hybrid composite. Photographic images of the B/K/epoxy hybrid composites and B/K/epoxy hybrid nanocomposites after the cone calorimetry test are shown in Fig. 12. It is clearly visible that hybrid nanocomposites have more char yield compared to B/K/epoxy. B/K/MMT and B/K/HNT yield a greyish char residue. The char yield by B/K/MMT covers relatively more area

compared to B/K/HNT. This explains the lower smoke property observed in B/K/MMT compared to B/K/HNT in this study. In contrast, B/K/OMMT yields a black thick char residue that covers almost the whole surface area. This indicates that the addition of OMMT induced better dispersion of nanoparticles within the epoxy matrix which enhanced the formation of a strong and compact carbonaceous structure. This correlates well with the TGA findings on B/K/OMMT recording the highest char combustion temperature (T_{max2}) among the composites. Another possible reason for this observation is the interaction between the amine ($-HN_2$) group of APTES and oxirane ring of epoxy monomer inducing high crosslink density.[29] This enhances the migration of nanoclay with an effective viscosity gradient at high temperatures compared to that caused by unmodified MMT and HNT. Hence, the formation of a thermally stable insulating char layer leads to a lower burning rate and lower generation of combustion products such as volatiles and smoke.

Conclusions

In this study, we conducted a comparative study on three types of nanoclay by incorporating MMT, HNT and OMMT nanoclays into bamboo/kenaf reinforced epoxy hybrid composite. The WAXS and FESEM revealed that OMMT/epoxy exhibits a more uniform morphology while B/K/MMT and B/K/HNT form heterogenous morphologies with large tactoid formation. The TOD stability shows that the initial decomposition temperature of nanoclay filled hybrid nanocomposites is slightly lower compared to the unfilled hybrid composite. However, the TOD stability of the hybrid nanocomposites surpasses B/K/epoxy in

a temperature range >300 °C. During continuous heating, migration of nanoclays to the surface of the composites forms an effective thermal barrier and delays the thermal decomposition process. Also, B/K/OMMT possesses better charring ability, which leads to the formation of a stable and compact carbonaceous structure that decomposes at a relatively higher temperature. The flammability properties of the hybrid nanocomposites were evaluated by UL94 horizontal burning, LOI, cone calorimetry and smoke density tester. All hybrid nanocomposites achieved an HB40 rating in the UL-94 horizontal burning test. With the addition of nanoclay, the LOI value increased from 20 to 28%. The char residue obtained from TGA analysis correlated well with the increase in LOI value. A high correlation coefficient ($R^2 = 0.8374$) between the LOI and char yield was obtained. The nanoclay filled hybrid nanocomposites had an overall better fire performance with lower pHRR, longer burning time with lower mass loss rate and lower fire load for total heat release. The smoke generation also significantly reduced with the addition of nanoclays. The improved TOD stability and flammability properties of nanoclay filled hybrid nanocomposites are attributed to the ability of better charring effects from the formation of an insulation barrier which limited the migration of mass and heat between the gas and solid phase during the combustion process. Organically modified MMT exhibited better performance compared to unmodified nanoclay due to better interaction between the nanoclay and the polymer matrix and achieved a better dispersion level with less agglomeration.

Conflicts of interest

There are no interests to declare.

Acknowledgements

Notes and references

1 *Natural Fiber Reinforced Composites Market | Growth, Trends, and Forecast*, 2019–2024, https://www.mordorintelligence.com/industry-reports/natural-fiber-reinforced-composites-market, accessed 7 August 2019.

2 E. S. Goda, K. R. Yoon, S. H. El-sayed and S. E. Hong, *Thermochim. Acta*, 2018, **669**, 173–184.

3 A. Dasari, Z.-Z. Yu, G.-P. Cai and Y.-W. Mai, *Prog. Polym. Sci.*, 2013, **38**, 1357–1387.

4 P. Khalili, K. Y. Tshai, D. Hui and I. Kong, *Composites, Part B*, 2017, **114**, 101–110.

5 D. Gao, R. Li, B. Lv, J. Ma, F. Tian and J. Zhang, *Composites, Part B*, 2015, **77**, 329–337.

6 Q. Liu, D. Wang, Z. Li, Z. Li, X. Peng, C. Liu, Y. Zhang and P. Zheng, *Materials*, 2020, **13**, 2145.

7 N. M. Stark, R. H. White, S. A. Mueller and T. A. Osswald, *Polym. Degrad. Stab.*, 2010, **95**, 1903–1910.

8 H. Lu and C. A. Wilkie, *Polym. Degrad. Stab.*, 2010, **95**, 2388–2395.

9 M. Sain, S. Park, F. Suhara and S. Law, *Polym. Degrad. Stab.*, 2004, **83**, 363–367.

10 J. Chen and J. Han, *Results Phys.*, 2019, **14**, 102481.

11 A. Toldy, G. Szebényi, K. Molnár, L. Tóth, B. Magyar, V. Hliva, T. Czigány, B. Szolnoki, A. Toldy, G. Szebényi, K. Molnár, L. F. Tóth, B. Magyar, V. Hliva, T. Czigány and B. Szolnoki, *Polymers*, 2019, **11**, 303.

12 L. Ahmed, B. Zhang, R. Shen, R. J. Agnew, H. Park, Z. Cheng, M. S. Mannan and Q. Wang, *J. Therm. Anal. Calorim.*, 2018, **132**, 1853–1865.

13 Y. Wang, C. Liu, X. Shi, J. Liang, Z. Jia and G. Shi, *Polym. Compos.*, 2019, **40**, 202–209.

14 X. Yue, C. Li, Y. Ni, Y. Xu and J. Wang, *J. Mater. Sci.*, 2019, **54**, 13070–13105.

15 A. A. Azeez, K. Y. Rhee, S. J. Park and D. Hui, *Composites, Part B*, 2013, **45**, 308–320.

16 M. Shahid Nazir, M. H. Mohamad Kassim, L. Mohapatra, M. A. Gilani, M. R. Raza and K. Majeed, in *Nanoclay Reinforced Polymer Composites*, ed. R. Boufid, M. Jawaid and A. Qaiss, Springer, Singapore, 2016, pp. 35–55.

17 O. Zabihi, M. Ahmadi, S. Nikafshar, K. Chandrakumar Preyeswary and M. Naebe, *Composites, Part B*, 2018, **135**, 1–24.

18 M. Rajaei, N. K. Kim, S. Bickerton and D. Bhattacharyya, *Composites, Part B*, 2019, **165**, 65–74.

19 M. A. El-Fattah, A. M. El Saeed, M. M. Dardir and M. A. El-Sockary, *Prog. Org. Coat.*, 2015, **89**, 212–219.

20 N. Raghavendra, H. N. Murthy, S. Firdosh, R. Sridhar, G. Angadi, K. V. Mahesh and M. Krishna, *Proc. Inst. Mech. Eng., Part N*, 2017, **231**, 34–42.

21 D. Xiao, Z. Li, X. Zhao, U. Gohs, U. Wagenknecht, B. Voit and D.-Y. Wang, *Appl. Clay Sci.*, 2017, **143**, 192–198.

22 F. Rafiee, M. Otadi, V. Goodarzi, H. A. Khonakdar, S. H. Jafari, E. Mardani and U. Reuter, *Composites, Part B*, 2016, **103**, 122–130.

23 M. H. Hasan, M. S. Mollik and M. M. Rashid, *Int. J. Adv. Des. Manuf. Technol.*, 2018, **94**, 1863–1871.

24 R. M. Shahroze, M. R. Ishak, M. S. Salit, Z. Leman, M. Chandrasekar, N. S. Z. Munawar and M. Asim, *J. Vinyl Addit. Technol.*, 2019, vnl.21736.

25 N. Saba, M. Jawaid, M. M. Alrashed and O. Y. Alothman, *J. Build. Eng.*, 2019, **25**, 100829.

26 E. Monteiro, S. Leao, M. Norton, M. G. Martins and A. F. Avila, in *2018 AIAA/ASCE/AHS/ASC Structures, Structural Dynamics, and Materials Conference*, American Institute of Aeronautics and Astronautics, Reston, Virginia, 2018.

27 S. S. Chee, M. Jawaid, M. T. H. Sultan, O. Y. Alothman and L. C. Abdullah, *Polym. Test.*, 2019, **79**, 106054.

28 S. S. Chee, M. Jawaid, M. T. H. Sultan, O. Y. Alothman and L. C. Abdullah, *J. Therm. Anal. Calorim.*, 2018, 1–9.

29 S. S. Chee and M. Jawaid, *Polym*, 2019, **11**, 2012.

30 S. S. Chee, M. Jawaid, M. T. H. Sultan, O. Y. Alothman and L. C. Abdullah, *Composites, Part B*, 2018, **163**, 165–174.

31 L. N. Carli, O. Bianchi, G. Machado, J. S. Crespo and R. S. Mauler, *Mater. Sci. Eng. C*, 2013, **33**, 932–937.

32 O. Shepelev and S. Kenig, *Handbook of Thermoset Plastics*, 2014, pp. 623–695.

33 H. Zhang, S. Tangparitkul, B. Hendry, J. Harper, Y. K. Kim, T. N. Hunter, J. W. Lee and D. Harbottle, *Chem. Eng. J.*, 2019, **355**, 797–804.

34 R. Berahman, M. Raiati, M. Mehrabi Mazidi and S. M. R. Paran, *Mater. Des.*, 2016, **104**, 333–345.

35 L. Madaleno, J. Schjødt-Thomsen and J. C. Pinto, *Compos. Sci. Technol.*, 2010, **70**, 804–814.

36 N. Stevulova, A. Estokova, J. Cigasova, I. Schwarzova, F. Kacik and A. Geffert, *J. Therm. Anal. Calorim.*, 2017, **128**, 1649–1660.

37 G. Ounoughene, O. Le Bihan, C. Chivas-Joly, C. Motzkus, C. Longuet, B. Debray, A. Joubert, L. Le Coq and J.-M. Lopez-Cuesta, *Environ. Sci. Technol.*, 2015, **49**, 5450–5457.

38 C. Yu, Y. Ke, X. Hu, Y. Zhao, Q. Deng, S. Lu, C. Yu, Y. Ke, X. Hu, Y. Zhao, Q. Deng and S. Lu, *Polymers*, 2019, **11**, 834.

39 J. M. Hwu, G. J. Jiang, Z. M. Gao, W. Xie and W. P. Pan, *J. Appl. Polym. Sci.*, 2002, **83**, 1702–1710.

40 W. Xie, Z. Gao, K. Liu, W.-P. Pan, R. Vaia, D. Hunter and A. Singh, *Thermochim. Acta*, 2001, **367–368**, 339–350.

41 L.-H. Lee, *J. Polym. Sci. - Part A Gen. Pap.*, 1965, **3**, 859–882.

42 X. Zhang, Y. Wu, H. Wen, G. Hu, Z. Yang and J. Tao, *Polym. Degrad. Stab.*, 2018, **156**, 125–131.

43 F. Kačík, P. Šmíra, D. Kačíková, V. Veľková, A. Nasswettrová and V. Vacek, *Carbohydr. Polym.*, 2015, **117**, 681–686.

44 R. Vanholme, B. Demedts, K. Morreel, J. Ralph and W. Boerjan, *Plant Physiol.*, 2010, **153**, 895–905.

45 F. X. Collard and J. Blin, *Renewable Sustainable Energy Rev.*, 2014, **38**, 594–608.

46 H. Alamri, I. M. Low and Z. Alothman, *Composites, Part B*, 2012, **43**, 2762–2771.

47 J. Lenża, K. Merkel and H. Rydarowski, *Polym. Degrad. Stab.*, 2012, **97**, 2581–2593.

48 N. A. Isitman and C. Kaynak, *Polym. Degrad. Stab.*, 2011, **96**, 2284–2289.

49 P. Yuan, F. Bergaya and A. Thill, in *Nanosized Tubular Clay Minerals Halloysite and Imogolite*, Elsevier, 2016, vol. 7, pp. 1–10.

50 D. C. O. Marney, L. J. Russell, D. Y. Wu, T. Nguyen, D. Cramm, N. Rigopoulos, N. Wright and M. Greaves, *Polym. Degrad. Stab.*, 2008, **93**, 1971–1978.

51 N. Hayeemasae, K. Waesateh, A. Masa and H. Ismail, *J. Eng. Sci.*, 2019, **15**, 1–10.

52 M. E. Mngomezulu, M. J. John, V. Jacobs and A. S. Luyt, *Carbohydr. Polym.*, 2014, **111**, 149–182.

53 S. R. Hostler, A. R. Abramson, M. D. Gawryla, S. A. Bandi and D. A. Schiraldi, *Int. J. Heat Mass Transfer*, 2009, **52**, 665–669.

54 J. S. Im, S. K. Lee, S. J. In and Y.-S. Lee, *J. Anal. Appl. Pyrolysis*, 2010, **89**, 225–232.

55 D. van Krevelen, *Polymer*, 1975, **16**, 615–620.

56 C.-L. Chiang and C.-C. M. Ma, *Eur. Polym. J.*, 2002, **38**, 2219–2224.

57 K. Benzarti and X. Colin, in *Advanced Fibre-Reinforced Polymer (FRP) Composites for Structural Applications*, Woodhead Publishing, 2013, pp. 361–439.

58 K. Sałasińska, M. Borucka, M. Celiński, A. Gajek, W. Zatorski, K. Mizera, M. Leszczyńska and J. Ryszkowska, *Adv. Polym. Technol.*, 2018, **37**, 2394–2410.

59 F. J. Mastral, E. Esperanza, P. Garciía and M. Juste, *J. Anal. Appl. Pyrolysis*, 2002, **63**, 1–15.

60 H. J. Kruger, W. W. Focke, W. Mhike, A. Taute, A. Roberson and O. Ofosu, *J. Fire Sci.*, 2014, **32**, 498–517.

61 A. Subasinghe, R. Das and D. Bhattacharyya, *Int. J. Smart Nano Mater.*, 2016, **7**, 202–220.

62 L. C. Hatanaka, L. Ahmed, S. Sachdeva, Q. Wang, Z. Cheng and M. S. Mannan, *Plast., Rubber Compos.*, 2016, **45**, 375–381.

63 L. Ahmed, B. Zhang, R. Shen, R. J. Agnew, H. Park, Z. Cheng, M. S. Mannan and Q. Wang, *J. Therm. Anal. Calorim.*, 2018, **132**, 1853–1865.

64 M. Sacristán, T. R. Hull, A. A. Stec, J. C. Ronda, M. Galià and V. Cádiz, *Polym. Degrad. Stab.*, 2010, **95**, 1269–1274.

65 M. J. John, in *Green Composites for Automotive Applications*, Elsevier, 2018, pp. 43–58.